

PCCP

Accepted Manuscript



This is an *Accepted Manuscript*, which has been through the Royal Society of Chemistry peer review process and has been accepted for publication.

Accepted Manuscripts are published online shortly after acceptance, before technical editing, formatting and proof reading. Using this free service, authors can make their results available to the community, in citable form, before we publish the edited article. We will replace this *Accepted Manuscript* with the edited and formatted *Advance Article* as soon as it is available.

You can find more information about *Accepted Manuscripts* in the [Information for Authors](#).

Please note that technical editing may introduce minor changes to the text and/or graphics, which may alter content. The journal's standard [Terms & Conditions](#) and the [Ethical guidelines](#) still apply. In no event shall the Royal Society of Chemistry be held responsible for any errors or omissions in this *Accepted Manuscript* or any consequences arising from the use of any information it contains.



Journal Name

ARTICLE

Preparation of $\text{TiO}_x\text{N}_y/\text{TiN}$ Composite for Photocatalytic Hydrogen Evolution under Visible Light

Tao Yang,^a Qun Li,^a Xiwang Chang,^a Kuo-Chih Chou,^a and Xinmei Hou^{*a}Received 00th January 20xx,
Accepted 00th January 20xx

DOI: 10.1039/x0xx00000x

www.rsc.org/

$\text{TiO}_x\text{N}_y/\text{TiN}$ heterojunction composite with tunable chamber structures were prepared through reduction and nitridation of organotitanium obtained via solvothermal alcoholysis at 900 °C for 4h in partial cracked NH_3 . Owing to the low synthesis temperature, $\text{TiO}_x\text{N}_y/\text{TiN}$ duplicates the original structure of the organotitanium. It also demonstrates an outstanding activity toward hydrogen production as high as $34.9 \mu\text{mol}\cdot\text{h}^{-1}\cdot\text{g}^{-1}$, which is about 1.5 times higher than the highest value reported in the literature for TiN material. The enhanced photoactivity can be ascribed to the heterojunction structure, which is beneficial for separating the photogenerated carriers in space.

Introduction

In recent years, energy shortages and environmental pollution have become the focus of world attention. As one of the most promising solutions for these problems, semiconductor photocatalysis has attracted much attention since they have important advantages just like green, safety and sustainability.^{1,2} To date, TiO_2 semiconductor has undoubtedly proven to be one of the excellent photocatalysts for water splitting and the oxidative decomposition of many organic compounds.³ However, due to its wide band-gap of 3.2 eV, TiO_2 can only be excited by ultraviolet or near-ultraviolet radiation, which occupies only 4% of the incoming solar light spectrum on the earth.⁴ To efficiently utilize the visible region ($\lambda > 400 \text{ nm}$) which covers the largest proportion of the solar spectrum, the development of visible-light-driven (VLD) photocatalysts is the current trend. During the past decade, various strategies including suitable textural design,⁵⁻⁷ doping,^{8,9} and forming a semiconductor heterojunction by combining metal and/or other semiconductors^{10,11} have been employed to improve the photocatalytic efficiency.

Titanium nitride (TiN) is an Fm3m cubic crystal containing both covalent and metallic bonds. And it has a narrow energy band gap (0.80 eV) and good electrical conductivity, which are beneficial to photocatalytic H_2 production. In recent work, Li *et al.*¹² developed a new approach to prepare pure TiN mesoporous microspheres with solid, yolk-shell and hollow chambers through NH_3 nitridation at 800 °C for 20 h. The yolk-shell TiN exhibited a high activity of $114 \mu\text{mol}\cdot\text{g}^{-1}$ over 5h in the visible light-induced photocatalytic water splitting to produce H_2 . Although TiN was used in photocatalytic H_2 production successfully, its application as a photocatalyst is limited

so far owing to the rapid recombination between photoelectrons and holes, which leads to low quantum efficiencies. The rapid recombination is attributed in part to the inherently high defect density of TiN and unfavourable band position for hydrogen reduction. To tackle the problem concerning low efficiency for hydrogen evolution from water splitting under the irradiation of solar light, different hybrid semiconductor heterostructures have been explored to promote greater separation of the photoinduced charge carriers. For example, $\text{TiO}_x\text{N}_y/\text{CdS}$ heterostructures were found to exhibit a high rate of photocatalytic decomposition of methanol when compared with either CdS or TiO_xN_y alone.¹³ C-N- TiO_2 ($\text{TiO}_x\text{N}_y/\text{TiO}_x\text{C}_y$) nanomaterials exhibited the highest photocatalytic activity of methylene blue degradation under visible light irradiation when compared with either N- TiO_2 (TiO_xN_y) or C- TiO_2 (TiO_xC_y).¹⁴ Titanium oxy nitride (TiO_xN_y) is developed for electrochemical applications because its specific properties can be tuned according to the N/O ratio. In particular, oxygen rich titanium oxy nitride has been widely used as photoelectrochemical devices,¹⁵ especially in solar selective absorbers to improve their performance under visible light.¹⁶⁻²⁰ In this work, TiO_xN_y can be applied as a sensitizer to enhance the photoactivity of TiN, which has not been reported before, to our knowledge.

Herein a semiconductor heterojunction composite of $\text{TiO}_x\text{N}_y/\text{TiN}$ was constructed combining solvothermal alcoholysis and reduction and nitridation. By controlling the solvothermal alcoholysis time, reaction temperature and holding time, $\text{TiO}_x\text{N}_y/\text{TiN}$ with solid, yolk-shell and hollow microspheres were prepared. Especially $\text{TiO}_x\text{N}_y/\text{TiN}$ heterojunction with yolk-shell structure demonstrated an outstanding activity toward H_2 production as high as $34.9 \mu\text{mol}\cdot\text{h}^{-1}\cdot\text{g}^{-1}$, which is about 1.5 times of the highest value reported in the literature for TiN material.

^aState Key Laboratory of Advanced Metallurgy, University of Science and Technology Beijing, Beijing 100083, China. E-mail: houxinmei@ustb.edu.cn

[†]Electronic Supplementary Information (ESI) available. See DOI: 10.1039/x0xx00000x

Theoretical calculation

The electronic structures of TiN and TiO_xN_y can be calculated by plane-wave-density function theory (DFT) using the Cambridge Serial Total Energy Package (CASTEP) program package (calculation conditions are listed in Table S1). The optimized simple crystal structures of TiN, Ti_2O_4 and TiO_xN_y with N doping concentration in the range of 0 to 33 mol% ($\text{Ti}_{16}\text{O}_{31}\text{N}$, $\text{Ti}_8\text{O}_{15}\text{N}$, $\text{Ti}_4\text{O}_7\text{N}$, $\text{Ti}_2\text{O}_3\text{N}$ and $\text{Ti}_2\text{O}_2\text{N}_2$) were calculated and the result is shown in Fig. S1. O in the symmetrical positions of rutile titanium dioxide (TiO_2) crystal cell has been substituted by N. According to the calculation result, TiN has a narrow energy band gap (0.80 eV) (Fig. 1a), which is in consistent with the result reported by Li's *et al.* group.¹² The calculated band gaps of TiO_xN_y decrease from 3.084 to 0.009 eV with N doping concentration increasing from 0 to 33 mol% (Fig. 1e). It can be seen that the band gap of TiO_xN_y is more than 0.8 eV when the doping concentration of N is less than 17 mol% (Fig. 1d ($\text{Ti}_2\text{O}_3\text{N}$, 0.918 eV)). The reason of changed band gaps of TiO_xN_y with N doping concentration is the introduction of new energy band. From the density of states showed in Fig. 1c-d, there is a newly formed energy band introduced by the 2p states of doping N. From above calculation, TiN combining with TiO_xN_y with proper N doping concentration is expected to form favorable band-edge position, which may be potential candidate for visible-light responsive photocatalyst.

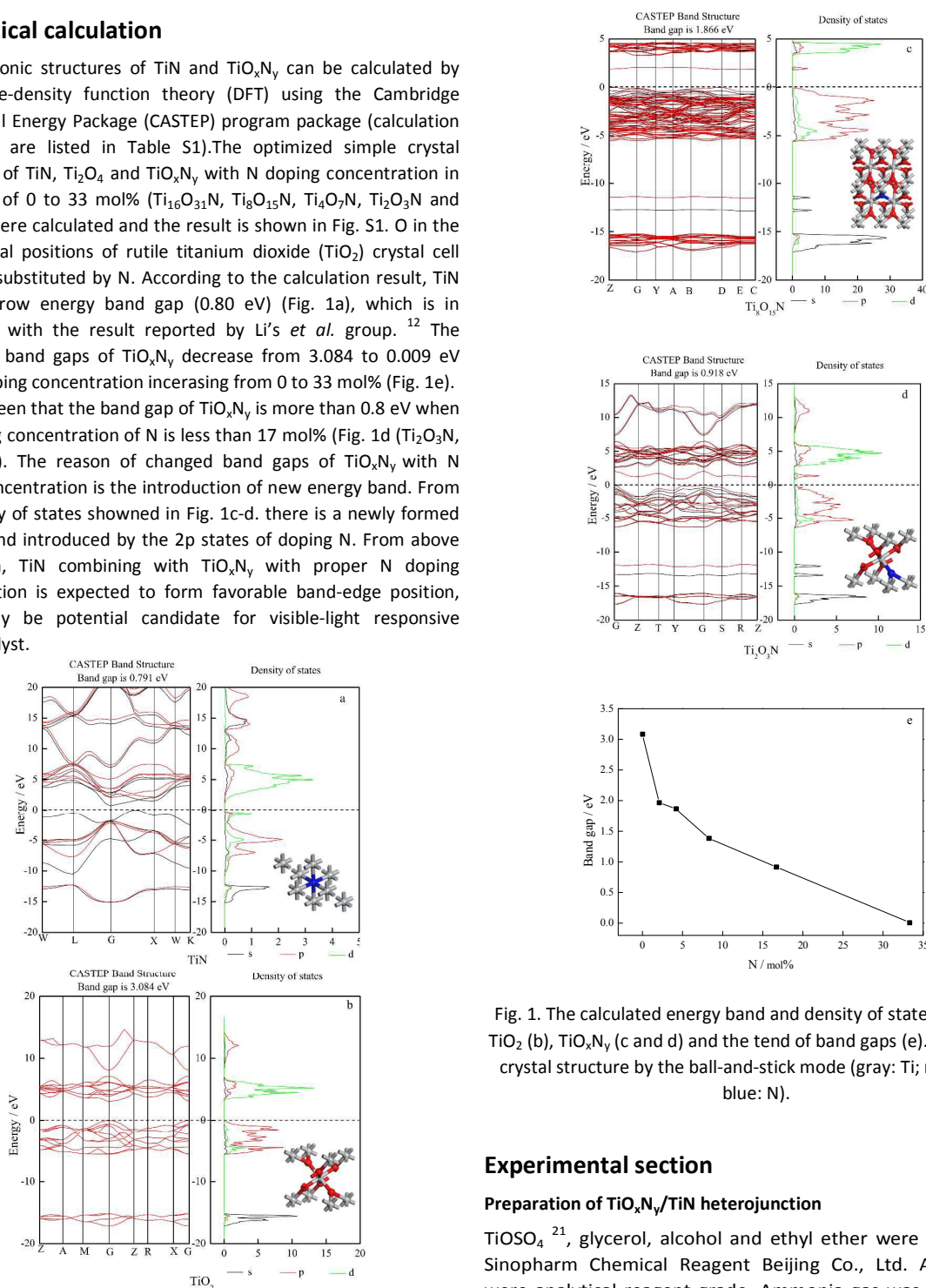


Fig. 1. The calculated energy band and density of states of TiN (a), TiO_2 (b), TiO_xN_y (c and d) and the trend of band gaps (e). Inset of the crystal structure by the ball-and-stick mode (gray: Ti; red: O; and blue: N).

Experimental section

Preparation of $\text{TiO}_x\text{N}_y/\text{TiN}$ heterojunction

TiOSO_4 ²¹, glycerol, alcohol and ethyl ether were supplied by Sinopharm Chemical Reagent Beijing Co., Ltd. All reagents were analytical reagent grade. Ammonia gas was supplied by Haipu Gas Co., Ltd. Deionized (DI) water was used in all experiments.

The synthesis procedure involved two sequential reaction steps: (1) the formation of TiO_2 precursor via solvothermal alcoholysis and (2) carbothermal reduction and nitridation of the precursor to obtain $\text{TiO}_x\text{N}_y/\text{TiN}$ powder. During the first procedure, TiOSO_4 in a solution containing glycerol, alcohol and ethyl ether with the volume ratio: 1: 10: 20: 8 was

adopted in the experiment. To obtain the product with solid, yolk-shell and hollow microspheres, the mixture was put in Teflon-lined stainless steel autoclave and heated at 110 °C for 1, 48 and 168 h respectively. When the temperature was cooled to room temperature, the product was filtered, washed thoroughly with alcohol and dried in oven at 110 °C for 12 h. The above TiO₂ precursors were placed into a porcelain boat and heated to 800-1000 °C for 2-5 h in following partial cracked NH₃ at the flow rate of 0.1 L/min. To duplicate the morphology of TiO₂, two steps are taken during the synthesis process, i.e. one is the low synthesis temperature. The other is to keep heating and cooling slowly during synthesis process.

Characterization

The obtained products were characterized with X-ray diffraction (XRD) with Cu K α radiation ($\lambda = 1.54178 \text{ \AA}$) (XRD, TTRIII, Rigaku). The accelerating voltage and the applied current were 40 kV and 40 mA respectively. The microstructures of the samples were examined by scanning electron microscopy (SEM, FEI Nova 230 Nano). Transmission electron microscopy (TEM) images were collected by using a JEOL model JEM 2010 EX microscope at an accelerating voltage of 200 kV. The optical properties of the samples were analyzed by UV-Vis diffuse reflectance spectroscopy (UV-Vis DRS) using a UV-Vis spectrophotometer (UV2250, Shimadzu), in which BaSO₄ was used as the background. The chemical states of TiO_xN_y/TiN composite was determined by X-ray photoelectron spectroscopy (XPS) in a VG Multilab 2009 system (UK) with a monochromatic Al K α source and charge neutralizer.

Photocatalytic tests.

Photocatalytic H₂ production was carried out in an air free closed gas circulation system reaction cell made of quartz. The total cylindrical volume of the cell was 200 mL. An optically polished piece of quartz glass was fused on top of the cell to minimize light scattering. Hydrogen evolution was detected using a gas chromatograph (Beijing, GC-3240, TCD, Ar carrier), which was connected to a gas-circulation line. Argon with a flow rate of 100 mL·min⁻¹ was used as a carrier gas, and was passed through the quartz glass cell.

In a typical photocatalytic experiment, 0.2 g of the prepared TiO_xN_y/TiN composites photocatalysts were dispersed under constant stirring in a 200 mL mixed solution of Na₂S (5 mL, 0.1 mol·L⁻¹), Na₂SO₃ (5 mL, 0.04 mol·L⁻¹) and distilled water (190 mL). The reaction was initiated by irradiation with a 300 W xenon lamp fitted with a cutoff filter ($\lambda > 420 \text{ nm}$). The whole system, including the photocatalyst, was flushed with Ar at 100 mL min⁻¹ for 1 h to remove any trace of air (including nitrogen and oxygen) before any photocatalytic reaction was carried out. During the process, agitation of the solution ensured uniform irradiation of the suspensions. A 0.4 mL sample of the generated gas was collected intermittently through the septum, and hydrogen content was analyzed by a gas chromatograph (GC-14C, Shimadzu, Japan, TCD, nitrogen as a carrier gas and 5 Å molecular sieve column). All glassware was

rigorously cleaned and carefully rinsed with distilled water prior to use.

Results and discussions

Crystal Phase Analyses

XRD patterns indicate the strong diffraction peaks of TiN corresponding to 36.90°, 42.86°, 62.24°, 74.61° and 78.48° (PDF 38-1420) in all the samples. The crystallization degree and purity of TiN increase with increasing nitridation temperature (Fig. 2a). The refinement of XRD data at different temperature (Table S2) indicates that the constant a increases from 4.216 (800 °C) to 4.241 Å (900 °C). This is between the theoretical value of TiO (4.180 Å) and TiN (4.241 Å),²² indicating the existence of TiO_xN_y. When the temperature reaches up to 950-1000 °C, the constant a is calculated to be 4.241 Å, which is in consistent with the standard value of TiN (PDF 38-1420 ($a = 4.241 \text{ \AA}$)).²³

In view of the effect of reaction time, the XRD patterns of the samples obtained at 900 °C for different reaction time at partial cracked NH₃ atmosphere are demonstrated in Fig. 2b. It can be seen that some small diffraction peaks of TiO₂ still exist when the reaction time is 3 h. With the nitridation time is extended to 4-5 h, all the characteristic peaks are indexed to be that of TiN. The refinement of XRD data at 900 °C for different time is also calculated as shown in Table S3. The constant a increases with the reaction time prolonging. When the nitridation time is 4 h, the constant a (4.238 Å) is between the theoretical value of TiO (4.180 Å) and TiN (4.241 Å), indicating the existence of TiO_xN_y. From above experiments, the synthesis condition of TiO_xN_y/TiN composite is selected as 900 °C for 4 h. Pure TiN can be produced at 1000 °C for 3 h.

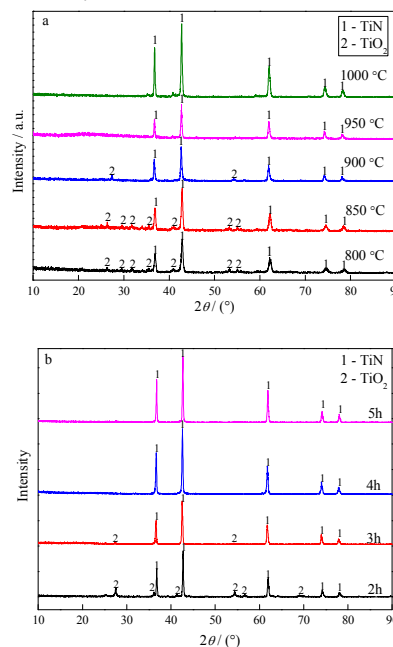


Fig. 2. XRD patterns of the obtained yolk-shell product synthesized at different conditions: (a) different temperature for 3 h (b) different time at 900 °C

XPS is adopted to further characterize $\text{TiO}_x\text{N}_y/\text{TiN}$ composite. The full XPS spectrum (Fig. 3(a)) of the samples obtained at 900°C for 4h shows the existence of C, N, Ti and O. Fine XPS spectra of Ti 2p, N 1s and O 1s are presented in Figs. 3 (b-d). The Ti 2p bands have three groups of peaks, i.e. the typical peaks for TiN (at 455.3 eV, 457.5 eV, 460.9eV and 463.0 eV), the peaks for TiO_xN_y (at 456.1 eV and 461.7 eV) and the peaks for TiO_2 (at 459.1 eV and 464.7 eV) (Fig. 3(b)).²²⁻²⁵ The existence of TiO_2 is attributed to the reaction of TiN and TiO_xN_y particles with oxygen from air atmosphere. From the XPS spectra of N 1s (Fig. 3(c)), the peak at 396.3 eV can be assigned to TiO_xN_y .^{22,23,26} The peak centred at 397.3 eV corresponds to Ti-N bond in TiN and peak at 399.2 eV corresponds to C≡N bond.²² The existence of C≡N mainly comes from the absorption of C from the atmosphere. From the XPS spectra of N 1s, the molar content of N in TiO_xN_y is about 6.8 mol%. XPS signals of O 1s (Fig. 3(d)) are observed at around 530.4 eV and 532.0 eV, which can be assigned to Ti-O bond in TiO_2 and TiO_xN_y respectively,^{22,23} indicating that the samples are composed of TiN and TiO_xN_y . The molar ratio of $\text{TiO}_x\text{N}_y/\text{TiN}$ is determined by XPS to be 15.64, corresponding to the mass content of TiN to be 95 mass%. Since the content of TiO_xN_y was too low to be detected by XRD, there are not the diffraction peaks of TiO_xN_y XRD patterns.

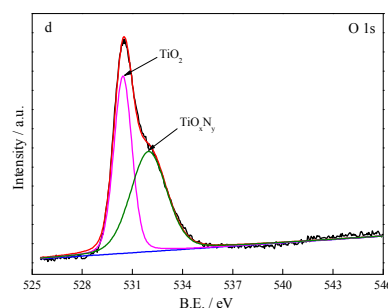
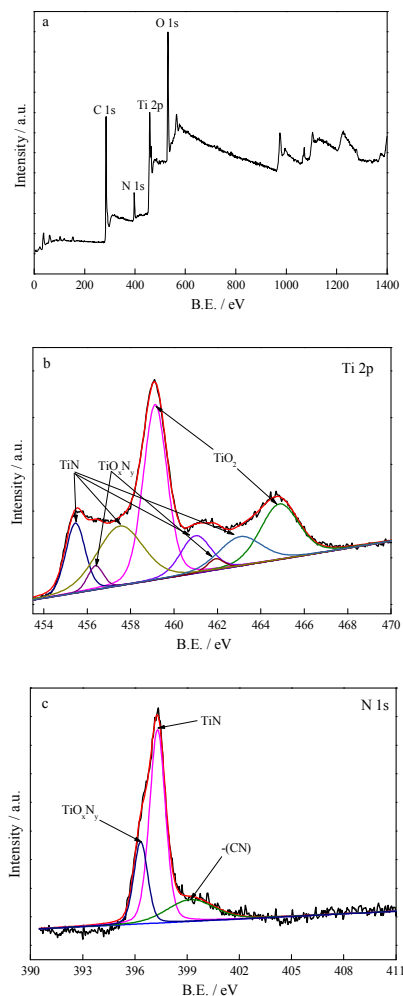


Fig. 3. The full spectrum of XPS of the samples obtained at 900°C for 4h (a), XPS spectra of (b) Ti 2p, (c) N 1s, (d) O 1s.

Microstructure Analyses

SEM images of $\text{TiN}/\text{TiO}_x\text{N}_y$ obtained at 900°C for 4h in partial cracked NH_3 are shown in Fig. 4. It can be seen that the microstructure of $\text{TiO}_x\text{N}_y/\text{TiN}$ nanoparticles duplicate the original structure of the precursors. The average diameter of $\text{TiO}_x\text{N}_y/\text{TiN}$ composite with solid microstructure is about 1-2 μm (Fig. 4b). Yolk-shell $\text{TiO}_x\text{N}_y/\text{TiN}$ are composed of a small yolk with an average diameter around 500 nm and a thin shell with an average thickness around 20 nm (Fig. 4d). The hollow microspheres are composed of a thin shell with an average diameter around 1-2 μm and an average thickness around 20 nm (Fig. 4f).

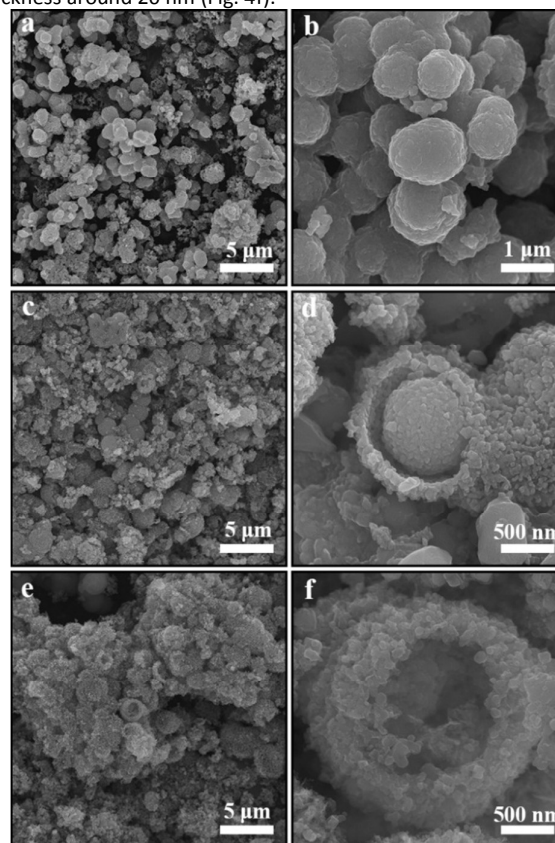


Fig. 4. SEM photographs of $\text{TiO}_x\text{N}_y/\text{TiN}$ composite: (a),(b) solid, (c),(d) yolk-shell, (e),(f) hollow

TEM images of $\text{TiO}_x\text{N}_y/\text{TiN}$ composite are shown in Fig. 5. The low-

magnification TEM images (Fig. 5a and b) show that $\text{TiO}_x\text{N}_y/\text{TiN}$ composite is composed of regular aggregated particles with coarse surfaces. The lattice-resolved HRTEM image (Fig. 5c) indicates that the lattice spacing is 0.25 nm and 0.40 nm, which is consistent with the (111) planes of cubic TiN and the (111) planes of TiO_xN_y , respectively. In addition, it can be seen that TiN crystal is in close contact with TiO_xN_y crystal to form a heterojunction, which is believed to promote the transfer of photogenerated electrons and holes between TiN and TiO_xN_y , suppresses their recombination, and thus enhances the photocatalytic activity.²⁷⁻²⁹

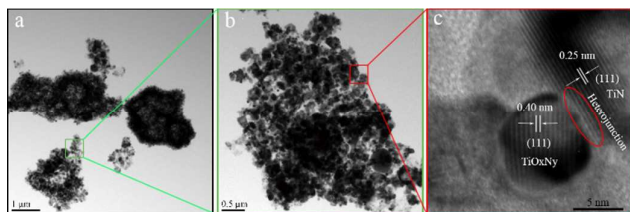


Fig. 5. TEM photographs of $\text{TiO}_x\text{N}_y/\text{TiN}$ composite
Photocatalytic activities

The water splitting of H_2O to H_2 performance of solid $\text{TiO}_x\text{N}_y/\text{TiN}$, yolk-shell $\text{TiO}_x\text{N}_y/\text{TiN}$ and hollow $\text{TiO}_x\text{N}_y/\text{TiN}$ samples under light irradiation was examined in the presence of Na_2S and Na_2SO_3 as a hole acceptor. For comparison, the photocatalytic H_2 production of TiN and TiO_xN_y (N/Ti=2) is also carried out respectively. TiN was synthesized at 1000 °C for 3 h in flowing partial cracked NH_3 . TiO_xN_y (N/Ti=2) were synthesized through a microemulsion-hydrothermal method using triethylamine, urea, thiourea and hydrazine as organic compounds³⁰. The mixture is put in Teflon-lined stainless steel autoclave and heated at 120°C for 12h. The results are shown in Fig. 6. By comparison, the as-prepared $\text{TiO}_x\text{N}_y/\text{TiN}$ heterojunction with yolk-shell and hollow structures exhibit better photocatalytic H_2 production activities while the maximum H_2 production rate is achieved for yolk-shell $\text{TiO}_x\text{N}_y/\text{TiN}$ with $35 \mu\text{mol}\cdot\text{h}^{-1}\cdot\text{g}^{-1}$. Li's *et al.* group reported that the yolk-shell TiN synthesized at 800 °C for 20 h showed the larger visible-light-driven photocatalytic hydrogen production to be $22.8 \mu\text{mol}\cdot\text{h}^{-1}\cdot\text{g}^{-1}$.¹² Our result is 1.5 times of that value. The stability tests are also investigated by carrying out recycling reactions three times for photocatalytic hydrogen production using yolk-shell $\text{TiO}_x\text{N}_y/\text{TiN}$ under visible light irradiation. No decrease in catalytic activity is observed in the recycling reactions as shown in Fig. 6 (b).

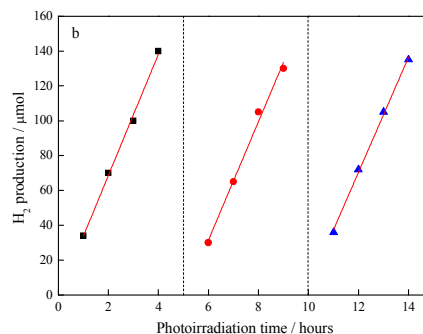
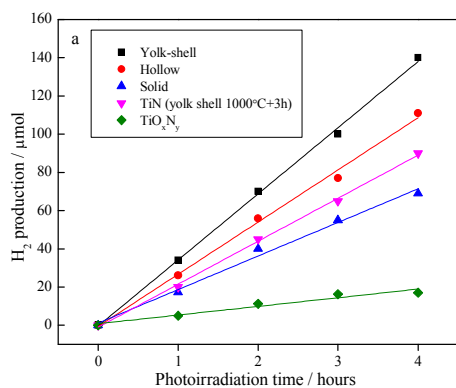


Fig. 6. a. Comparison of H_2 production rates of TiN, TiO_xN_y and $\text{TiO}_x\text{N}_y/\text{TiN}$ heterojunction with different nanostructure; b. Recycling test of the yolk-shell $\text{TiO}_x\text{N}_y/\text{TiN}$ in the photocatalytic H_2 evolution.

The enhanced photocatalytic hydrogen production performance of the yolk-shell $\text{TiO}_x\text{N}_y/\text{TiN}$ heterojunction are attributed to the formation of heterojunction by TiN and TiO_xN_y with the proper electronic structures and its special nanostructures. From the theoretical calculation as shown in Fig.1, TiN combining with TiO_xN_y with proper N doping concentration is expected to form favorable band-edge position, which may be potential candidate for visible-light responsive photocatalyst. From XPS spectra, the molar content of N in TiO_xN_y is about 6.8 mol%, corresponding to the band gap of 1.56 eV. When TiN and TiO_xN_y is combined together, the band gap should in the range of 0.8 and 1.56 eV. UV-Vis diffuse reflection spectra (Fig. S2) is also carried out. The absorption band-edge for yolk-shell $\text{TiO}_x\text{N}_y/\text{TiN}$ are at about 850 nm, corresponding to band gap energy to be 1.4 eV, verifying the theoretical calculation. Under visible-light irradiation, the photogenerated electrons are excited from the valence bands (VBs) to the conduction bands (CBs) of TiN and TiO_xN_y in the $\text{TiO}_x\text{N}_y/\text{TiN}$ composite, creating positive holes in VB of TiN and TiO_xN_y (Fig.7a). Since CB (-0.6eV)¹² level of TiN is lower than that of TiO_xN_y (CB -0.4eV)³¹, electrons in CB of TiN can be transferred to that of TiO_xN_y . The VB (0.2eV)¹² level of TiN is lower than that of TiO_xN_y (VB 0.6-1.1eV)³¹, holes in VB of TiO_xN_y can be transferred to that of TiN. Therefore, the probability of electron-hole recombination can be reduced, which can be confirmed by the photoluminescence spectra (Fig. 7b). It is found that $\text{TiO}_x\text{N}_y/\text{TiN}$ exhibits a fluorescence decrease (or quenching) as compared with TiN and TiO_xN_y ³⁰, indicating that the photogenerated carrier recombination is inhibited greatly. These results should be derived from the intimate contacts between TiN and TiO_xN_y . Finally, the sacrificial reagents are oxidized by the positive holes in the surface of TiN and the photo-excited electrons in the surface of TiO_xN_y can generate hydrogen, and thus the photocatalytic reaction can be enhanced greatly.³²

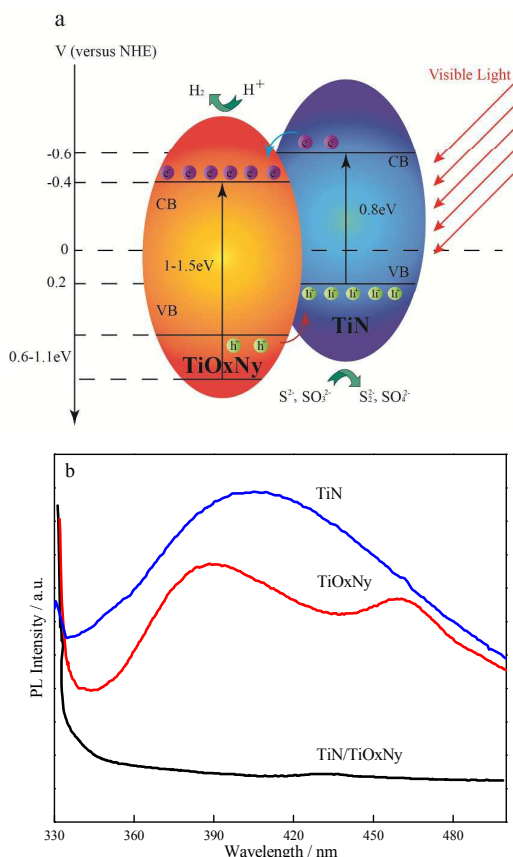


Fig. 7. (a) Schematic diagram of photocatalytic mechanism for $\text{TiO}_x\text{N}_y/\text{TiN}$, (b) Photoluminescence spectra of $\text{TiO}_x\text{N}_y/\text{TiN}$

In addition to the electronic structures, the special yolk-shell nanostructures is another important factor for the enhancement of the photocatalytic activities. On the one hand, the specific surface area of yolk-shell nanostructure are increased significantly, which increase the aqueous suspension contact area. On the other hand, the resulting yolk-shell nanostructures may result in the multiple light reflections within the chamber, which leads to efficient photocatalytic and photoelectro-chemical performances.

Conclusions

$\text{TiO}_x\text{N}_y/\text{TiN}$ heterojunction composite with solid, yolk-shell and hollow microspheres were prepared through reduction and nitridation of organotitania obtained via solvothermal alcoholysis. Especially, the yolk-shell $\text{TiO}_x\text{N}_y/\text{TiN}$ heterojunction demonstrated an outstanding activity toward H_2 production as high as $34.9 \mu\text{mol}\cdot\text{h}^{-1}\cdot\text{g}^{-1}$, which was about 1.5 times of the value reported in the literature. The enhanced activity toward H_2 production is attributed to the combined effect of the electronic structures of heterojunction and the yolk-shell morphology. This work is applicable to the development of multiphase structures in various semiconductors with controllable morphology for applications in solar energy conversion, gas sensors and photoluminescence.

Acknowledgements

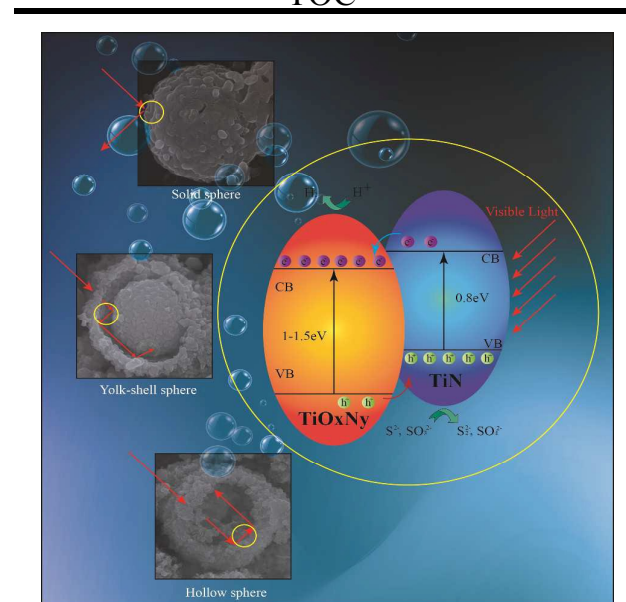
The authors express their appreciation to the New Century Excellent Talents in University (No. NECT-12-0779), the National Science Fund for Excellent Young Scholars of China (No. 51522402) and the Program for Changjiang Scholars and Innovative Research Team in University (No. IRT1207) for financial support.

Notes and references

- W. Lubitz and W. Tumas, *Chem. Rev.*, 2007, **107**, 3900-3903.
- A. Fujishima, X. Zhang and D. A. Tryk, *Int. J. Hydrogen Energy*, 2007, **32**, 2664-2672.
- M. Fujihira, Y. Satoh and T. Osa, *Nature*, 1981, **293**, 206-208.
- C. Chen, W. Cai, M. Long, B. Zhou, Y. Wu, D. Wu and Y. Feng, *ACS Nano*, 2010, **4**, 6425-6432.
- D. Jing, M. Liu, Q. Chen and L. Guo, *Int. J. Hydrogen Energy*, 2010, **35**, 8521-8527.
- X. Wang, K. Maeda, X. Chen, K. Takanabe, K. Domen, Y. Hou, X. Fu and M. Antonietti, *J. Am. Chem. Soc.* 2009, **131**, 1680-1681.
- D. Wang, A. Pierre, M. G. Kibria, K. Cui, X. Han, K. H. Bevan, H. Guo, S. Paradis, A. R. Hakima and Z. Mi, *Nano. Lett.* 2011, **11**, 2353-2357.
- F. Meng, J. Li, Z. Hong, M. Zhi, A. Sakla, C. Xiang and N. Wu, *Catal. Today*, 2013, **199**, 48-52.
- S. Li, L. Zhang, T. Jiang, L. Chen, Y. Lin, D. Wang and T. Xie, *Chem-Eur. J.* 2014, **20**, 311-316.
- Y. Bi, H. Hu, S. Ouyang, Z. Jiao, G. Lu and J. Ye, *J. Mater. Chem.*, 2012, **22**, 14847-14850.
- H. Wang, S. Li, L. Zhang, Z. Chen, J. Hu, R. Zou, K. Xu, G. Song, H. Zhao, J. Yang and J. Liu, *CrystEngComm*, 2013, **15**, 9011-9019.
- G. Li, P. Zhang, Z. Bian, J. Zhu, L. Wu and H. Li, *ChemSusChem* 2013, **6**, 1461-1466.
- K. Prabakar, T. Takahashi, T. Nezuca, K. Takahashi, T. Nakashima, Y. Kubota and A. Fujishima, *J. Vac. Sci. Technol. A*, 2007, **25**, 1188-1192.
- D. Chen, Z. Jiang, J. Geng, Q. Wang and D. Yang, *Ind. Eng. Chem. Res.* 2007, **46**, 2741-2746.
- Y. Kuroda, T. Mori, K. Yagi, N. Makihata, Y. Kawahara, M. Nagao and S. Kittaka, *Langmuir*, 2005, **21**, 8026-8034.
- S. Sato, R. Nakamura and S. Abe, *Appl. Catal. A: Gen.* 2005, **284**, 131-137.
- M. Bellardita, M. Addamo, A. Di Paola, L. Palmisano and A. M. Venezia, *Phys. Chem. Chem. Phys.* 2009, **11**, 4084-4093.
- H. Wu and Z. Zhang, *Int. J. Hydrogen Energy*, 2011, **36**, 13481-13487.
- B. S. Huang and M. Y. Wey, *Int. J. Hydrogen Energy*, 2011, **36**, 9479-9486.
- K. H. Kim and S. H. Lee, *Thin Solid Films*, 1996, **283**, 165-170.
- A. K. Sinha, S. Jana, S. Pande, S. Sarkar, M. Pradhan, M. Basu, S. Saha, A. Pal and T. Pal, *CrystEngComm*, 2009, **11**, 1210-1212.
- M. Drygas, C. Czosnek, R. T. Paine and J. F. Janik, *Chem. Mater.* 2006, **18**, 3122-3129.
- M. Zúkalová, J. Procházka, Z. Bastl, J. Duchoslav, L. Rubáček, D. Havlíček and L. Kavan, *Chem. Mater.*, 2010, **22**, 4045-4055.
- K. Prabakar, T. Takahashi, T. Nezuca, T. Nakashima, Y. Kubota and A. Fujishima, *J. Vac. Sci. Technol., A* 2006, **24**, 1156-1160.
- A. Trenczek-Zajac, M. Radecka, K. Zakrzewska, A. Brudnik, E. Kusior, S. Bourgeois, M. C. Marco de Lucas, L. Imhoff, *J. Power Sources*, 2009, **194**, 93-103.
- C. Di Valentin, E. Finazzi, G. Pacchioni, A. Selloni, S. Livraghi, M. C. Paganini and E. Giamello, *Chem. Phys.*, 2007, **339**, 44-56.

- 27 C. Mondal, A. Singh, R. Sahoo, A. K. Sasmal, Y. Negishi and T. Pal, *New J. Chem.*, 2015, **39**, 5628-5635.
- 28 J. Yu, J. Zhang and S. Liu, *J. Phys. Chem. C*, 2010, **114**, 13642–13649.
- 29 J. G. Yu and B. Wang, *Appl. Catal. B*, 2010, **94**, 295–302.
- 30 Y. Cong, J. Zhang, F. Chen and M. Anpo, *J. Phys. Chem. C*, 2007, **111**, 6976-6982.
- 31 W. Wang, O. Savadogo and Z. F. Ma, *Int. J. Hydrogen Energ.* 2012, **37**, 7405-7417.
- 32 H. Wang, L. Zhang, Z. Chen, J. Hu, S. Li, Z. Wang, J. Liu and X. Wang, *Chem. Soc. Rev.*, 2014, **43**, 5234-5244.

TOC



TiO_xN_y/TiN heterojunction composite with tunable chamber structures were prepared. It demonstrates an outstanding activity toward H₂ production as high as 34.9 μmol·h⁻¹·g⁻¹.